JOURNAL OF NANOMATERIALS AND APPLICATIONS

Journal of Nanomaterials and Applications

Journal homepage: https://jna.com.vn

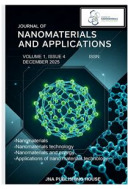

A state of the art review on MoS_2 preparations and applications

Ştefan ŢĂLU [1], Vu Van Thu [2], Nguyen Dac Dien [3,*]

[1,] Technical University of Cluj-Napoca, The Directorate of Research, Development and Innovation, Management (DMCDI), Constantin Daicoviciu Street, no. 15, Cluj-Napoca, 400020, Cluj county, Romania.

[2, 3,] Faculty of Occupational Safety and Health, Vietnam Trade Union University, Hanoi, 100000, Vietnam.

Review info

Type of articles:
Review article

Corresponding author*:
Nguyen Dac Dien:
diennd@dhcd.edu.vn

Received: 27 December 2025
Revised: 07 February 2026
Accepted: 04 April 2026
Published: 18 April 2026

Abstract: Molybdenum disulfide (MoS_2) has emerged as a promising two-dimensional material for applications in energy storage and environmental remediation due to its unique layered structure and tunable electronic properties. However, a comprehensive understanding of the relationship between synthesis strategies, defect engineering, and performance remains limited. This review critically evaluates various synthesis approaches, including top-down and bottom-up methods, and correlates them with structural characteristics such as layer thickness, morphology, and defect density. Comparative analysis indicates that hydrothermal methods provide optimal scalability and cost efficiency, while chemical vapor deposition ensures superior crystallinity. However, limitations such as low conductivity and aggregation remain critical challenges.

Keywords: MoS_2; synthesis methods; defect engineering; energy storage; photocatalysis; nanomaterials

1. Introduction

MoS_2, a representative transition metal dichalcogenide, has attracted extensive attention owing to its tunable electronic structure and rich physicochemical properties. These characteristics enable MoS_2 to serve as a versatile platform for applications ranging from energy storage and catalysis to environmental remediation and biomedicine [1-4]. MoS_2 comprises stacked monolayers held together by weak van der Waals forces and strong S-Mo-S covalent bonds connecting the Mo and S atoms. MoS_2 exists in several crystalline phases, including 1T, 2H, and 3R, each exhibiting distinct electronic and catalytic properties. The metallic 1T phase provides high electrical conductivity, whereas the semiconducting 2H and 3R phases offer superior stability, making phase engineering a key strategy for tailoring MoS_2 toward

specific applications [5-7]. The electronic structure of MoS_2 strongly depends on its thickness, evolving from an indirect bandgap in bulk to a direct bandgap in monolayer form due to quantum confinement effects. This transition significantly enhances light absorption and carrier dynamics, enabling promising optoelectronic and photoelectrochemical applications [8-10]. The 1T phase exhibits superior performance in electrochemical reactions, while the 2H phase is not conductive to electrochemical energy storage [11]. The nanostructure of MoS_2 includes 0D (quantum dots), 1D (nanotubes, nanorods), 2D (nanosheets), and 3D (flowers, cubes). MoS_2 quantum dots (QDs) exhibit a high electron transfer, high activity, n-type semiconductor characteristic. The size distribution of MoS_2 QDs is relatively narrow between 1 nm and 7 nm, with an average diameter of 3.6 nm [12]. MoS_2 nanotubes have a diameter of about 200 nm and an average length of a few microns [13]. MoS_2 microspheres feature a hollow spherical shell, approximately 200 nm in diameter [14]. MoS_2 nanosheets have a large specific surface area, generating numerous electrochemical reaction active sites. They tend to agglomerate during material preparation or electrochemical reactions and diminish electrochemical performance. Nanostructure, porous structure and hollow structure can increase the reactive site and specific surface area, reduce the diffusion distance of electrolyte ions, and improve the stability of electrode materials [15]. The maximum specific surface area of porous structure is limited to 100 m^2/g [16]. The hollow structure can expose more electrochemically active atoms and improve the stability of the electrode material circulation [17].

In addition, in recent years, several research groups have successfully studied many factors affecting the structure, phase transformation, crystallization of CuNi [18], AgAu [19] alloys and their applications [20]. The obtained results show that there is a great influence of doping concentration, atomic number, temperature, etc. on their properties. This review focuses on the synthesis methods and applications of MoS_2 nanostructures such as nanosheets, nanospheres, nanoflowers, etc. in energy storage devices, catalysis, wastewater treatment through adsorption, photocatalysis, membrane filtration and antibacterial activity. Although numerous studies have reported the synthesis and applications of MoS_2, a comprehensive understanding of the interdependence between preparation methods, structural features, and application performance remains insufficient. In particular, the trade-offs among scalability, structural controllability, and functional efficiency have not been systematically analyzed. This review aims to bridge this gap by critically evaluating recent advances in MoS_2 preparation and applications, highlighting current limitations and future research directions. Despite extensive research on MoS_2 synthesis and applications, existing review articles primarily focus on individual preparation techniques or specific application domains. A systematic correlation between preparation strategies, resulting structural features, and application-oriented performance remains insufficiently addressed. Despite significant progress, existing review studies mainly focus on either synthesis methods or individual applications without establishing a clear relationship between structure, defects, and performance. In particular, the effects of layer number, morphology, and defect density on functional efficiency have not been systematically analyzed. This limitation restricts the rational design of MoS_2-based materials. Therefore, this review aims to establish a comprehensive framework linking synthesis strategies to structural features and application performance. The structure of this review is organized as follows: Section 2 discusses synthesis methods, Section 3 presents characterization techniques, Section 4 reviews applications, and Section 5 outlines future research directions. This work provides a unified structuredefect–performance framework that has not been systematically reported in previous reviews.

2. Preparation methods

2.1. Mechanical stripping method

The top-down method involves the conversion of bulk materials into a single layer or a few layers of MoS_2 nanostructures by breaking down the block MoS_2 material's interlayer van der Waals force under the influence of outside forces. Each of the top down stripping techniques has its benefits and drawbacks. Mechanical stripping is a technique that uses weak bonding between layers to peel off large crystals layer by layer to form 2D material. The adhesive of transparent tape delaminates crystals into a sheet. Single or multi-layer nanosheets retained on the substrate can be obtained by stripping the transparent tape [21]. The mechanical peeling method can produce 1-4 layers of MoS_2 with varying thickness. However, the mechanical stripping method finds it challenging to meet the needs of large scale production in industrial practical applications and substrate contamination impacts film quality that is not suitable for biomedical applications [22].

2.2. Liquid phase stripping method

This method separates bulk crystals into single or multi layer 2D structures within water or organic solvents by ultrasonic or shear forces. The solvent molecules can weaken the interaction between the material layers that are separated into individual layers under ultrasonic action. The weak van der Waals forces between MoS_2 layers enable it to be decomposed into several layers or single layers by acoustic processing. The nanosheets obtained through liquid phase stripping exhibit excellent dispersion and stability in water. This method has a higher yield than the mechanical stripping approach. However, this method uses high ultrasonic energy that often results in the production of small sized nanosheets. Organic solvents used in liquid phase ultrasonic stripping can lead to environmental contamination, so have few practical uses [23].

2.3. Ion-intercalation method

This method inserts small-radius cations such as alkali metal ions (Li^+, Na^+, K^+) between bulk material layers, weakening the interlayer van der Waals interaction force. The covalent bonds present within the same layer, while van der Waals forces of interaction maintain the different layers in layered materials. Ions of suitable size enable them to be inserted into the spaces between layers. When lithium reacts with water to produce hydrogen gas which encourages stripping [24]. In the electrochemical intercalation approach, the experimental setup involves a graphite cathode and a lithium anode, a MoS_2 block material serving as the active material. The thickness and size of MoS_2 nanosheets can be altered by varying the electrode voltage. However, this method cannot produce large area MoS_2 nanosheets or separate multilayer nanosheets into single layer MoS_2. This process requires a prolonged reaction time and the organic intercalation compounds used are prone to explosion [25].

2.4. Hydrothermal/Solvothermal method

The bottom up approach was characterized by its ability to prepare large-area nanosheets and has attracted widespread attention. Through the growth of atoms and molecules, this method enables the synthesis of nanoparticles with precise shape, size, and chemical composition [26]. The hydrothermal/solvothermal process occurs in a high-temperature sealed autoclave to yield the desired material. This method can produce large-scale MoS_2 powders or thin film nanostructures. By controlling reaction time, temperature, pH, and precursors, we can synthesize MoS_2 with various morphologies such as nanoflowers, nanosheets or nanotubes. The pressure in the reactor can be controlled by adjusting the heating temperature and the volume ratio of the liquid to the reactor tank. This method does not necessitate specialized procedures or equipment, suitable for large-scale production [27].

2.5. Physical vapor deposition (PVD) method

It is a solid gas solid phase conversion process, including evaporation, sputtering under vacuum condition into gaseous atoms, molecules, ions, then nucleation and growth process on the target substrate through the low-pressure deposition. The crystal growth can be controlled through regulating temperature, temperature gradient, evaporation temperature, concentration, gas flow, etc. MoS_2 powder was used as precursor, Ar as the carrier gas, the temperature was maintained at 900°C in the evaporation region of the source material and 650°C in the growth region of the target substrate. However, the PVD method can only be applied to produce thin layer MoS_2 [28].

2.6. Chemical vapor deposition (CVD) method

CVD method is used to prepare 2D layered MoS_2 and MoS_2-based heterostructures with large scale, high purity, high crystallinity, controllable morphology, adjustable thickness, and minimum structural defect. CVD technology deposits gaseous chemicals on the substrate surface, the precursor reacts or decomposes on the substrate material under vacuum and high temperature conditions to achieve 2D MoS_2. The thickness, size and morphology of MoS_2 film can be controlled by adjusting the deposition parameters such as gas flow rate, growth temperature, growth time, pressure, precursor types, and substrate materials [29]. The CVD process is typically carried out in a tubular furnace, the prepared substrate (SiO_2) is positioned at one end of the furnace, the precursor (sulfur powder or H_2S, MoO_3 powder) is placed at the opposite end, Ar is used as a carrier gas, the product is 2D MoS_2 with the transverse size in the range of 10-30 nm [30]. The type of precursor can be chosen based on the material properties, however, the high reaction temperature makes it difficult to use traditional flexible substrates for making thin film devices in many applications. CVD and PVD enable the preparation of few-layer or single-layer nanosheets with controllable form and structure. They are suitable for growing large areas of MoS_2. However, their disadvantages are time consumption and high cost. Hydrothermal and solvothermal methods are often used for electrode preparation because of their low cost. Although diverse preparation methods have been developed, no single approach simultaneously fulfills scalability, precise structural control, and cost efficiency. Mechanical and liquid-phase exfoliation are advantageous for laboratory-scale studies, while hydrothermal and solvothermal methods offer scalable routes for electrochemical applications. In contrast, CVD and PVD techniques enable high-quality film growth but remain constrained by high cost and processing complexity [29, 30].

Table 1 Comparison of MoS_2 synthesis methods in terms of layer control, defect control, cost, scalability, and applications.

Method	Layer Control	Defect Control	Cost	Scalability	Application
Mechanical exfoliation	Excellent	Low	High	Poor	Research
Liquid exfoliation	Moderate	Medium	Medium	Moderate	Coatings
Ion intercalation	Moderate	High	High	Low	Few-layer
Hydrothermal	Moderate	Moderate	Low	High	Energy
CVD	Excellent	Excellent	High	Moderate	Electronics

As summarized in Table 1, hydrothermal synthesis provides the best trade-off between cost and scalability, making it suitable for large-scale applications, whereas CVD offers superior crystallinity but suffers from high operational costs. Notably, defect density varies significantly across synthesis methods and plays a critical role in determining electrochemical and catalytic performance.

3. Characterizations

Figure 1a shows the scanning electron microscope (SEM) images of flower-like MoS_2 microspheres. The thickness of MoS_2 nanosheets is tens of nm, this structure has a large specific surface area. SEM image of MoS_2 microsphere depicts hollow spherical shell with 2-4 μm in diameter (Figure 1b). Figure 1c is the TEM image of MoS_2 nanotube with a diameter of about 15 nm and the length of hundred nanometers. Figure 1d is the SEM image of MoS_2 microrods with diameter ranging from about 5-10 μm and length of around 100 μm. Three morphologies of MoS_2 structure are micro-nano structure, porous structure, and hollow structure. The micro-nano structures possess limited specific surface area, the porous structure can greatly increase the specific surface area but its maximum specific area is limited to 100 m^2/g, the hollow structure possesses the highest specific surface area. The thickness, porosity, shape, and size of hollow structure can be adjusted to give various surface properties. The ultraviolet-visible (UV-Vis) absorption spectra of semiconducting (S-MoS_2) (Figure 2a) shows two absorption bands at 613 and 660 nm due to the energy splitting from the valence band spin-orbital coupling with wide lateral dimension. Another absorption band at 442 nm is due to the quantum effect of small lateral-sized MoS_2 nanosheets. On the other hand, the absorption spectrum of M-MoS_2 has no absorption band but a monotonic change, showing its metallic property [31]. Figure 2b shows the photoluminescence (PL) spectra from the bilayer and monolayer of the MoS_2 flake on the SiO_2/Si substrate, the photoluminescence (PL) emission peak located at 675 nm, the PL intensity gradually decreases with increasing film thickness, the quantum yield drops rapidly from monolayer to bilayer due to rotational stacking disorder [32].

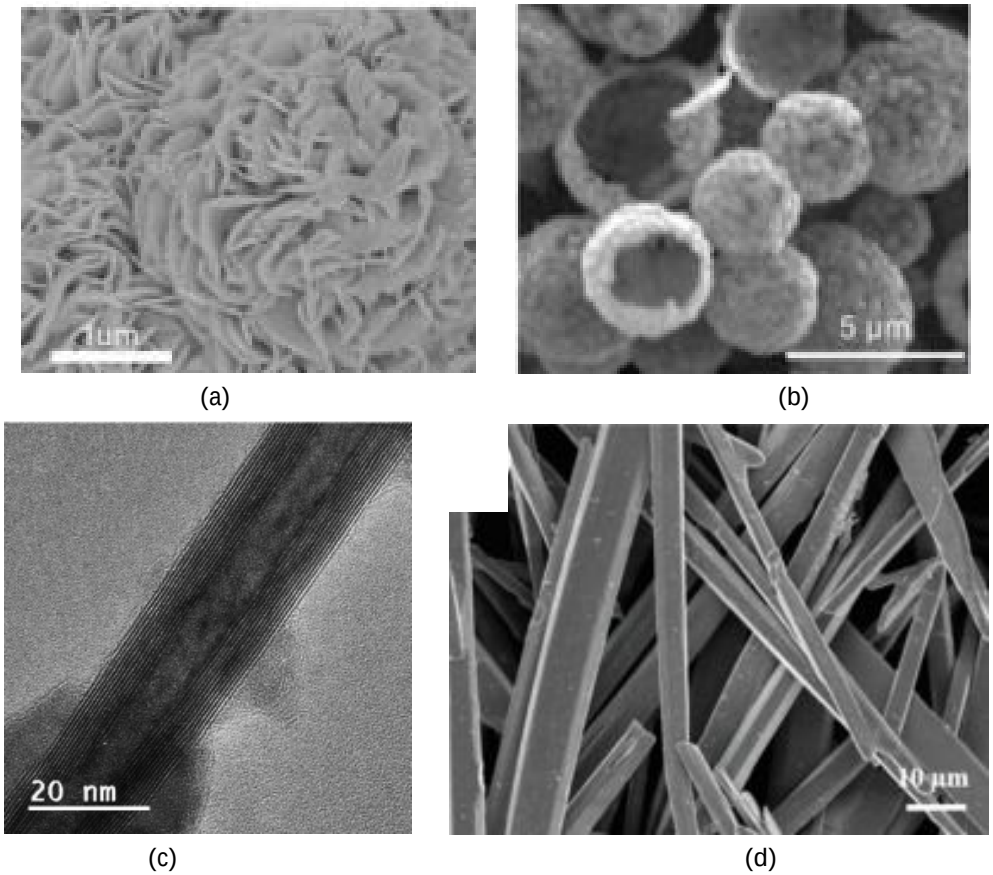

(a) (b)

(c) (d)

Figure 1. SEM images of flower-like MoS_2 microspheres [34] (a), hollow MoS_2 microsphere [14] (b), TEM image of MoS_2 nanotube [35] (c), SEM image of MoS_2 microspheres [36] (d).

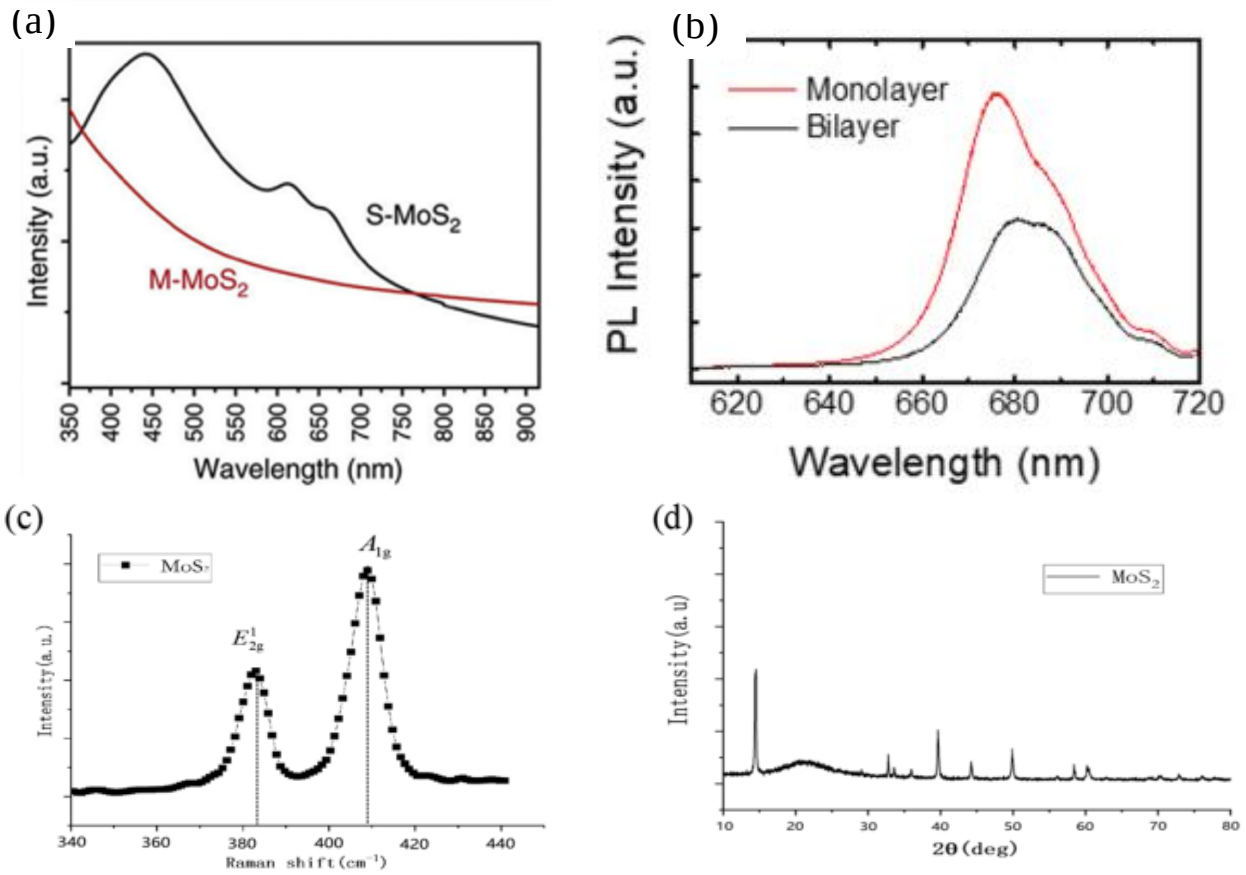

Figure 2. UV–Vis spectra (a) [9], PL spectra (b) [32], Raman spectra (c), XRD pattern(d) [33]

The results confirm the layered structure and crystallinity of MoS_2 materials. The optical and structural analyses confirm the layered structure and crystallinity of MoS_2. Figure 2c shows the Raman spectrum of MoS_2 nanosheets. Two Raman characteristic bands appeared at 385 and 419 cm^{-1} corresponding to the in-plane E^1_{2g} and out-of-plane A_{1g} vibration modes of MoS_2 [33]. This parameter is crucial for tuning the electronic structure and catalytic performance of MoS_2 The difference between the E_2g^1 and A_1g peaks can be used to estimate the number of layers, with larger separation indicating thicker layers. XRD peak broadening is associated with reduced crystallite size and increased defect density, which directly affects electrochemical performance. Figure 2d depicts the X-ray diffraction (XRD) pattern of MoS_2 nanosheets. Two intense peaks at 2θ of 14.1° and 40° correspond to the (002) and (100) planes of MoS_2 [33]. Beyond phase identification, characterization techniques provide essential insights into defect density, layer number, and interlayer coupling, which directly influence charge transport and electrochemical behavior. Establishing structure–performance correlations through these techniques is therefore critical for rational MoS_2 material design [31-33].

Energy-dispersive X-ray spectroscopy (EDS) was used in identifying the elemental composition of material. The EDS spectrum of MoS_2 nanoflowers in Figure 3a confirmed the appearance of S and Mo with the weight percentages of 44.27% and 55.73%, respectively [37]. High-resolution transmission electron microscopy (HRTEM) image (Figure 3b) shows distinct lattice fringes of 0.27 nm with 60° angles attributed to the (100) and (010) planes of MoS_2 [38].

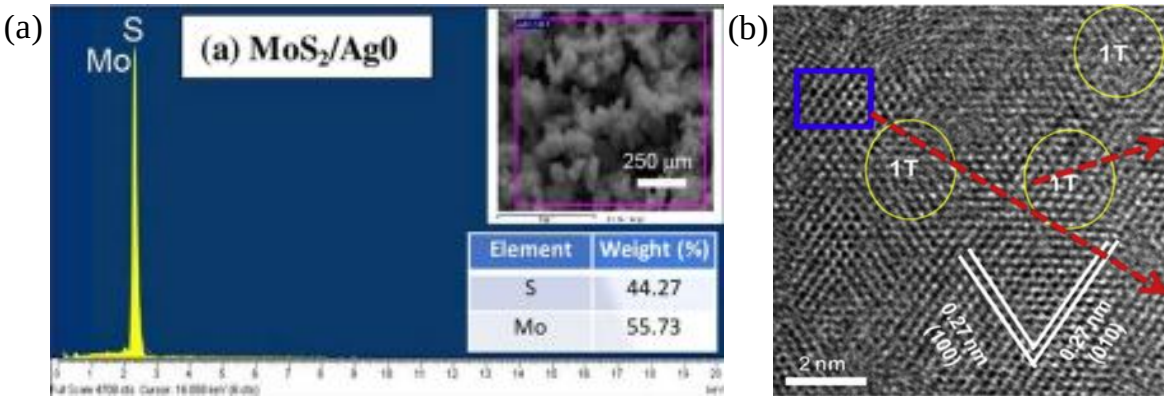

Figure 3. EDS spectrum of MoS_2 nanoflowers [37] (a), HRTEM of MoS_2 nanosheets [39] (b).

These characterization techniques are essential for establishing the relationship between structure and performance to ion diffusion mechanisms, charge transport efficiency, and catalytic activities, which are crucial in practical applications.

4. Applications of MoS_2

4.1. Energy storage applications

MoS_2 has been extensively investigated as an electrode material for lithium-ion and sodium-ion batteries owing to its layered structure, large interlayer spacing, and multiple redox-active sites. However, pristine MoS_2 suffers from intrinsic limitations such as low electrical conductivity and severe volume variation during repeated charge–discharge processes. To overcome these challenges, various material design strategies, including conductive matrix integration, defect engineering, and heterostructure construction, have been widely employed to enhance charge transport and structural stability. As a result, MoS_2-based composite electrodes generally exhibit improved specific capacity, rate capability, and cycling performance compared with pristine MoS_2. Overall, these advances demonstrate that rational structural and compositional engineering is critical for unlocking the full electrochemical potential of MoS_2 in energy storage applications [40-44]. Despite promising performance, MoS_2 electrodes suffer from low electrical conductivity and volume expansion during cycling. Compared to bulk MoS_2, nanosheet structures exhibit significantly higher specific capacity due to increased active surface area.

4.2. Supercapacitor

Supercapacitor is a high-capacity electrochemical capacitor, working as a fast charging energy storage device. The main shortcomings of supercapacitors in practical application are low energy density and high production cost [45]. MoS_2 is prone to fracture or agglomeration during charge and discharge, reducing the stability of the electrode cycle. Combining carbon-based materials with MoS_2 using the synergistic effect between two materials can improve the electrochemical activity of MoS_2 [46]. 3D MoS_2 nanospheres with the help of carbon quantum dots can facilitate the insertion of ions into the MoS_2 layers and improve the structural stability of the electrode material [47]. The addition of oxygen in MoS_2 increases the interlayer spacing of electrolyte diffusion and reduces the band gap of charge transfer, which is conducive to the mass transfer of electrolyte. The 3D nanostructure exposes the material to more active sites and pores, provides a larger specific surface area and improves ion diffusion in electrochemical processes [48]. MoS_2 grown on conductive substrates such as Ni foam and carbon cloth provides a low-resistance channel for ion transport, accelerates ion diffusion and improves cycle stability. MoS_2 grown by Ni foam has a large specific surface area and many active sites which improve the

electrochemical performance of electrode materials [49]. In MoS_2/Fe_2O_3 composite, Fe_2O_3 can supply more active sites, facilitate faster electrolyte ion migration to the nanocomposite, enhance reaction rate, and encourage capacitance growth. While MoS_2 promotes the cycle of the electrode material, improves the electron transfer dynamics, shortens the electron transfer channel, and increases the electron transfer capacity [50]. The nanosheet array offers abundant exposed electroactive sites which facilitate the insertion and removal of ions. The robust interface between MoS_2 and Ni_3S_2/Co_4S_3 eases the shrinkage and expansion of the volume during rapid charge and discharge, resulting in excellent conductivity and cycle stability [51]. Layered structures formed by combining MoS_2 with carbon material, conductive polymer or metal oxide possess the improved specific surface area and charge transfer, expose more reactive sites, reduce the diffusion distance of electrolyte ions, and improve the stability of electrode materials. Composites of MoS_2 nanostructures with carbon-based materials can develop high-performance energy storage electrode materials [52]. However, the surface energy of MoS_2 is large, making it easy to stack and agglomerate, thereby reducing the activity. The performance strongly depends on electron transport and interlayer spacing optimization. However, their long-term cycling stability remains inferior to carbon-based materials.

4.3. Wastewater treatment

Untreated effluents from various sources (domestic, municipal, mining, industry, agriculture, pharmaceutical) contain a wide range of toxic organic (dyes, pharmaceutical by-products and ingredients, pesticides, surfactants, polyaromatic hydrocarbons, fertilizers, phenols, etc.) that enter into the freshwater reservoirs and groundwater to take part in water pollution, which is dangerous for the human, animals and marine creatures living on the planet. Therefore, significant efforts have been made in water conservation and removing the toxic contaminants from water effluents before discharging them into the water bodies or for consumption. MoS_2 nanomaterials have been applied in cleaning the wastewater through adsorption, photocatalysis, membrane filtration and antibacterial activity. MoS_2 exhibits unique properties, such as high active surface area, low cost, small band gap, and the possibility of surface functionalization. MoS_2 and MoS_2-based nanocomposites showed excellent absorbents and photocatalysts to remove water contaminants [52]. S atoms on the MoS_2 surface can adsorb the cationic water contaminants through Lewis acid and base interaction. $MXene/NH_2@MoS_2$ facilitates hierarchical porous structure formation and the specific area of 8.27 m^2/g, leads to adsorption capacities of 1170 mg/g for malachite green (MG) and 1050 mg/g for crystal violet (CV) [53]. Electrostatic interaction between the cationic dye and negative MoS_2 was the major driven force for the adsorption. Magnetic Fe_3O_4/MoS_2 nanocomposites exhibited the maximum adsorption capacity for Congo red (CR) of 71 mg/g from aqueous medium [54]. The high absorption capacity towards cationic dyes is the effect of the van der Waals forces and the electrostatic interactions. However, the adsorption of anionic contaminants was compelled by van der Waals interaction. MoS_2 can also remove inorganic heavy metal ions owing to electrostatic interaction, complexation formation, and ion-exchange [55]. The MoS_2 surface exhibits a negative charge with positive counter ions which allows the metal-sulfur bond to form complexation. Multilayer adsorption involves the inner layer complex and outer layer complex formation. The metal ions can intercalate into the MoS_2 nanosheets to widen the interlayer spacing to expose the interior sulfur atoms and help the adsorption of metal ions. MoS_2 nanosheets can quickly adsorb Hg (I) with a capacity of 2506 mg/g [56]. MoS_2 has also been used for the adsorption of oil and organic solvents from the water. Hydrophobic interactions are the major forces for the adsorption of hydrophobic oils and organic

solvents on the MoS_2 surface [57]. Photocatalytic degradation of water contaminant molecules can clean wastewater without producing secondary waste. This advanced oxidation process exhibits several advantages such as cost-effectiveness, complete mineralization, simple practice, and mild reaction conditions [58]. Bulk MoS_2 exhibits a narrow band gap of ~ 1.3 eV, allowing the adsorption of most of the solar spectrum. However, the small band gap is responsible for the quick recombination of the photoinduced electron and hole pairs that negatively impact on its photocatalytic reaction. Few-layered 2D MoS_2 nanosheets or single-layered MoS_2 possess the larger band gap to improve the lifespan of charge carriers to participate in the photocatalytic reaction [59]. MoS_2 doped with metal or non-metal and MoS_2-based heterojunction can produce hydrogen through photocatalytic reaction using solar energy [60]. PPy@MoS_2 composite exhibits high photoactivity in degrading methylene blue (MB) with decomposition efficiency of 99.3%. Its high specific surface area and a remarkable heterostructure interface easily separate holes and electrons to improve the photodegradation ability [61]. MoS_2 nanoflowers, prepared through a hydrothermal method and thermally treated under Ag gas, were integrated with tetra(4-carboxyphenyl) porphyrin (TCCP) to form hybrid photocatalyst which achieved 95.72% Rhodamine B (RhB) degradation within 75 min under simulated sunlight. This enhanced efficiency stems from inorganic-organic interface contact that leads to superior charge separation and transfer [62]. Adsorption capacity can exceed 1000 mg/g for certain dyes. The adsorption mechanism is primarily governed by electrostatic interactions and surface complexation.

4.4. Membrane filtration

MoS_2 can be used to make nanoporous membranes and layer stacked membranes with specific pore sizes for wastewater treatment. These membranes act as a barrier for contaminants to block the passage of unwanted species and are driven by pressure, thermal, osmosis, and electrical forces. Nanoporous membranes are made using a few layers or single-layer MoS_2 nanosheets. Tannic acid-MoS_2 nanosheets/calcium silicate hydrate filtration system reaches the separation efficiency for methylene blue (MB) of 99.6%. The high filtration efficiency is due to the adjustment of the interlayer spacing and surface charge modification as well as the synergistic effect of electrostatic adsorption by the nanofiltration membrane and calcium silicate hydrate [63]. MoS_2 quantum dots doped with ZnO nanoparticles showed a significant rejection performance against Rhodamine B (RhB) (> 95%) owing to the synergistic effect of the quantum dots and semiconductor [64]. Cellulose acetate-MoS_2 nanocomposite membrane achieved oil removal rate as high as 83.12% over an 80-minute filtration [65]. The cross-linked polyvinyl alcohol (PVA) was intercalated between MoS_2 nanosheets, the composite displayed good rejection achieving 91.6 and 96.4% of methylene blue (MB) and direct red 80 (DR80), respectively [66].

4.5. Antibacterial activity

MoS_2 was functionalized to improve its application as an antibacterial agent. MoS_2 nanosheets prevent bacterial multiplication via physical contact or penetrate into the cell wall of bacteria to kill them. The photo-response of MoS_2 nanostructures helps in antibacterial activity due to the generation of reactive oxygen species (ROS) on the MoS_2 surface. The antibacterial properties of MoS_2 follow a three-step mechanism: direct physical contact, damage to the bacterial membrane, and create a disturbance in the microbial redox reaction process. MoS_2 spherical nanoparticles with an approximate diameter of 40 nm have been used as a promising material for antibacterial agents against Escherichia coli (E.coli) [67]. MoS_2 has been extensively explored as potent antibacterial agents to protect against antibiotic-resistant bacterial infections owing to its unique physical and chemical properties, including its large surface area,

high biocompatibility, biodegradability, strong light absorption, and low cytotoxicity [68]. MoS_2 has the potential to combat microbial infections through membrane disruption, reactive oxygen species (ROS) generation. The performance can be enhanced by combining MoS_2 with metals, carbon-based materials, or biocompatible polymers [69]. MoS_2 nanosheets and nanoflowers possess high surface area, provide much space for physical contact and oxidative stress to the bacterial cells, which help in bacterial death. An S-scheme WO_{3-x}/MoS_2 heterojunction photocatalytic system coupled with micro-nano bubbles has been developed for solar-powdered water disinfection. WO_{3-x}/MoS_2 achieved 94.23% inactivation of Escherichia coli (E. coli) and 93.09% of Staphylococcus aureus (S. aureus) within 20 min under simulated solar irradiation [70]. The Bi/MoS_2 heterojunction demonstrated outstanding antibacterial efficacy within 10-minute exposure to 808 nm near-infrared light. It effectively eradicated S. aureus through the synergistic action of photo-thermal effects and ROS generation under NIR irradiation [71]. Despite promising laboratory-scale performance, most MoS_2-based systems still face challenges related to long-term stability, material aggregation, and large-scale integration. Addressing these limitations requires deeper mechanistic understanding and scalable fabrication strategies tailored to specific application environments. The structure–performance relationship of MoS_2 is summarized in Table 2.

Table 2: Structure–performance relationship of MoS_2 nanostructures in different applications.

Application	Structure	Advantage	Limitation
Battery	Nanosheets	High capacity	Expansion
Supercapacitor	Porous	High surface	Stability
Wastewater	Nanoflowers	Adsorption	Aggregation

5. Future Research Directions

Future research should focus on defect engineering, heterostructure design, and scalable synthesis methods. Advanced techniques such as in situ characterization and machine learning-assisted design are expected to significantly enhance material performance. In addition, artificial intelligence and machine learning approaches are expected to play an important role in predictive material design.

6. Conclusion

MoS_2 has been synthesized by various methods, including mechanical stripping, liquid phase stripping, ion-intercalation, hydrothermal/solvothermal, CVD, PVD methods. The electronic structure of MoS_2 can be regulated by designing the layered structure (3D, porous, hollow, etc.) and by regulating growth methods. MoS_2 nanoflowers, nanospheres, nanotubes, nanorods, nanosheets have been characterized by TEM, SEM, XRD, EDS, UV-Vis, PL, Raman, and HRTEM. MoS_2 possesses potential applications in high-performance energy storage devices such as LIBs, SIBs, and supercapacitors. Introducing defects or doping heteroatoms to MoS_2 can produce active sites and coordination effects, improve ion mobility, increase the effective contact area between electrode materials and dielectrics, and improve the conductivity of the material. However, to achieve practical application of MoS_2 in the energy sector, the focus of future research should be the development of pore size structure and surface which is more conductive to ion transport, simulation calculation to explore the mechanism and law of multi-component MoS_2 composite to meet the needs of actual energy storage. MoS_2 has also been applied in wastewater treatment through adsorption, photocatalysis, membrane filtration and antibacterial activity. Therefore, the MoS_2 and MoS_2 based-composites are promising materials for environmental and

biological applications. Future research should focus on precise phase engineering, defect-controlled synthesis, and scalable fabrication of MoS_2-based materials. In addition, integrating advanced characterization with in situ techniques will be essential for uncovering structure–performance relationships. These findings provide a theoretical and practical foundation for the rational design of next-generation MoS_2-based materials.

Funding: The authors declare that no funds, grants, or other support were received during the preparation of this manuscript.

Data Availability Statement: The data that support the findings of this study are available from the corresponding authors upon reasonable request.

Declaration of competing interest: The authors declare that they have no known competing financial interest or personal relationships that could have appeared to influence the work reported in this paper.

References

[1] L. Liu, W. Wu, Y. Fang, H. Liu, F. Chen, M. Zhang, Y. Qin, (2021). Functionalized MoS_2 nanoflowers with excellent near-infrared photothermal activities for scavenging of antibiotic resistant bacteria, Nanomaterials 11, 2829. http://dx.doi.org/10.3390/nano11112829

[2] S. Gaba, M. Sahu, N. Chauhan, U. Jain, (2025). Unlocking the potential of low-dimensional MoS_2 as a smart nanoplatform for environmental technologies, therapeutic strategies, and biomedical sensing, Talanta Open 12, 100498. https://doi.org/10.1016/j.talo.2025.100498

[3] G. Anushya, M. Benjamin, R. Sarika, J.C. Pravin, R. Sridevi, D. Nirmal, (2024). A review on applications of molybdenum disulfide material: Recent developments, Micro and Nanostructures 186, 207742. https://doi.org/10.1016/j.micrna.2023.207742

[4] O. Samy, A. El Moutaouakil, (2021). A review on MoS_2 energy applications: recent developments and challenges, Energies 14, 4586. https://doi.org/10.3390/en14154586

[5] R.J. Toh, Z. Sofer, J. Luxa, D. Sedmidubský, M. Pumera, (2017). 3R phase of MoS_2 and WS_2 outperforms the corresponding 2H phase for hydrogen evolution, Chemical Communications 53, 3054-3057. https://doi.org/10.1039/C6CC09952A

[6] J. Sun, Z. Zhang, G. Lian, Y. Li, L. Jing, M. Zhao, D. Cui, Q. Wang, H. Yu, C.-P. Wong, (2022). Electron-injection and atomic-interface engineering toward stabilized defected 1T-rich MoS_2 as high rate anode for sodium storage, ACS Nano 16, 12425-12436. https://doi.org/10.1021/acsnano.2c03623

[7] S. Manzeli, D. Dumcenco, G. Migliato Marega, A. Kis, (2019). Self-sensing, tunable monolayer MoS_2 nanoelectromechanical resonators, Nature Communications 10, 4831. https://doi.org/10.1038/s41467-019-12795-1

[8] A. Kuc, T. Heine, (2015). The electronic structure calculations of two-dimensional transition-metal dichalcogenides in the presence of external electric and magnetic fields, Chemical Society Reviews 44, 2603-2614. https://doi.org/10.1039/C4CS00276H

[9] Y. Jiao, A.M. Hafez, D. Cao, A. Mukhopadhyay, Y. Ma, H. Zhu, (2018). Metallic MoS_2 for high performance energy storage and energy conversion, Small 14, 1800640. https://doi.org/10.1002/smll.201800640

[10] X. He, R. Wang, H. Yin, Y. Zhang, W. Chen, S. Huang, (2022). 1T-MoS_2 monolayer as a promising anode material for (Li/Na/Mg)-ion batteries, Applied Surface Science 584, 152537. https://doi.org/10.1016/j.apsusc.2022.152537

[11] Y. Gao, S. Wang, B. Wang, Z. Jiang, T. Fang, (2022). Recent progress in phase regulation, functionalization, and biosensing applications of polyphase MoS_2, Small 18, 2202956. https://doi.org/10.1002/smll.202202956

[12] A. Bayou, B. Asbani, Y. Doubi, N. Rajput, A. Campos, M. El Marssi, M. Jouiad, (2025). Superior photoelectrochemical performance of electrodeposited 1T/2H–MoS_2 quantum dots for hydrogen evolution, International Journal of Hydrogen Energy 139, 107-115. https://doi.org/10.1016/j.ijhydene.2025.05.233

[13] Y. He, J. Lan, S. Qu, M. Ma, Y. Zheng, X. Zheng, S. Guo, S. Huang, S. Li, J. Kang, (2024). Photocatalytic activity of molybdenum disulfide nanotube arrays with different wall thicknesses under visible light, Physics Letters A 520, 129734. https://doi.org/10.1016/j.physleta.2024.129734

[14] Y. Zhang, Y. Zhao, J. Li, L. Li, Y. Liu, B. Li, D. Li, X. Li, (2019). Facile strategy for controllable synthesis of hierarchical hollow MoS_2 microspheres with enhanced photocatalytic properties, Journal of Alloys and Compounds 784, 330-338. https://doi.org/10.1016/j.jallcom.2019.01.051

[15] R. Su, X. Zhu, L. Li, Z. Dong, (2025). Research progress of MoS_2-based electrode materials in electrocatalytic hydrogen evolution: from synthesis, characterization to electrocatalytic performance optimization strategy, International Journal of Hydrogen Energy 137, 26-72. https://doi.org/10.1016/j.ijhydene.2025.04.390

[16] H. Liu, Y. Lei, Y. Lin, L. Zhang, Y. Lu, (2020). One-pot Hydrothermal Synthesis of MoS_2 Porous Nanospheres and Their Electrochemical Properties, International Journal of Electrochemical Science 15, 1942-1948. https://doi.org/10.20964/2020.03.17

[17] M. Yu, C. Li, Z. Zheng, H. Yu, A. Xu, J. Wang, Y. Zhang, P. Dong, Z. Zhang, (2025). Construction of hollow nanospheres of MoS_2 as negative electrode material for sodium-ion and potassium-ion batteries, Electrochimica Acta 537, 146839. https://doi.org/10.1016/j.electacta.2025.146839

[18] D.N. Trong, V.C. Long, (2021). Factors affecting the depth of the Earth's surface on the heterogeneous dynamics of $Cu_{1-x}Ni_x$ alloy, x= 0.1, 0.3, 0.5, 0.7, 0.9 by molecular dynamics simulation method, Materials Today Communications 29, 102812. https://doi.org/10.1016/j.mtcomm.2021.102812

[19] T.T. Quoc, P.N. Dang, D.N. Trong, V.C. Long, Ş. Ţălu, (2023). Molecular dynamics study influence of factors on the structure, phase transition, and crystallization of the $Ag_{1-x}Au_x$, x= 0.25, 0.5, 0.75 alloy, Materials Today Communications 37, 107119. https://doi.org/10.1016/j.mtcomm.2023.107119

[20] U. Sarac, V.M. Thoai, D.N. Truong, S. Talu, (2025). Nanomaterial-based environmental sensors integrated with PLC control for smart livestock farming applications, Journal of Nanomaterials and Applications 1, 53-65. https://doi.org/10.65273/hhit.jna.2025.1.011

[21] N. Abid, A.M. Khan, S. Shujait, K. Chaudhary, M. Ikram, M. Imran, J. Haider, M. Khan, Q. Khan, M. Maqbool, (2022). Synthesis of nanomaterials using various top-down and bottom-up approaches, influencing factors, advantages, and disadvantages: A review, Advances in Colloid and Interface Science 300, 102597. https://doi.org/10.1016/j.cis.2021.102597

[22] Y. Huang, Y.-H. Pan, R. Yang, L.-H. Bao, L. Meng, H.-L. Luo, Y.-Q. Cai, G.-D. Liu, W.-J. Zhao, Z. Zhou, (2020). Universal mechanical exfoliation of large-area 2D crystals, Nature Communications 11, 2453. https://doi.org/10.1038/s41467-020-16266-w

[23] A. Gupta, V. Arunachalam, S. Vasudevan, (2016). Liquid-phase exfoliation of MoS_2 nanosheets: the critical role of trace water, The Journal of Physical Chemistry Letters 7, 4884-4890. https://doi.org/10.1021/acs.jpclett.6b02405

[24] A. Manthiram, X. Yu, S. Wang, (2017). Lithium battery chemistries enabled by solid-state electrolytes, Nature Reviews Materials 2, 16103. https://doi.org/10.1038/natrevmats.2016.103

[25] S. Wang, W. Li, J. Xue, J. Ge, J. He, J. Hou, Y. Xie, Y. Li, H. Zhang, Z. Sofer, (2024). A library of 2D electronic material inks synthesized by liquid-metal-assisted intercalation of crystal powders, Nature Communications 15, 6388. https://doi.org/10.1038/s41467-024-50697-z

[26] N. Srivastava, M. Srivastava, P.K. Mishra, V.K. Gupta. Green synthesis of nanomaterials for bioenergy applications. John Wiley & Sons Ltd; 2021.

[27] F. Wang, G. Li, J. Zheng, J. Ma, C. Yang, Q. Wang, (2018). Hydrothermal synthesis of flower-like molybdenum disulfide microspheres and their application in electrochemical supercapacitors, RSC Advances 8, 38945-38954. https://doi.org/10.1039/C8RA04350G

[28] J. Tao, J. Chai, X. Lu, L.M. Wong, T.I. Wong, J. Pan, Q. Xiong, D. Chi, S. Wang, (2015). Growth of wafer-scale MoS_2 monolayer by magnetron sputtering, Nanoscale 7, 2497-2503. https://doi.org/10.1039/c4nr06411a

[29] A. Singh, A.K. Mishra, (2025). Orientation dependent thermal behavior of CVD grown few layer MoS_2 films, Physica B: Condensed Matter 697, 416738. https://doi.org/10.1016/j.physb.2024.416738

[30] D. Mouloua, A. Kotbi, G. Deokar, K. Kaja, M. El Marssi, M.A. El Khakani, M. Jouiad, (2021). Recent progress in the synthesis of MoS_2 thin films for sensing, photovoltaic and plasmonic applications: a review, Materials 14, 3283. https://doi.org/10.3390/ma14123283

[31] X. Geng, W. Sun, W. Wu, B. Chen, A. Al-Hilo, M. Benamara, H. Zhu, F. Watanabe, J. Cui, T.-p. Chen, (2016). Pure and stable metallic phase molybdenum disulfide nanosheets for hydrogen evolution reaction, Nature Communications 7, 10672. https://doi.org/10.1038/ncomms10672

[32] B. Birmingham, J. Yuan, M. Filez, D. Fu, J. Hu, J. Lou, M.O. Scully, B.M. Weckhuysen, Z. Zhang, (2018). Spatially-resolved photoluminescence of monolayer MoS_2 under controlled environment for ambient optoelectronic applications, ACS Applied Nano Materials 1, 6226-6235. https://doi.org/10.1021/acsanm.8b01422

[33] X. Jiang, J. Cheng, P. Liu, Q. Gao, L. Liu, (2022). Facile preparation of four-layer MoS_2 nanosheets and their applications to organic light-emitting diode, Nanoscale Research Letters 17, 87. https://doi.org/10.1186/s11671-022-03726-z

[34] J. Liu, P. Xu, J. Liang, H. Liu, W. Peng, Y. Li, F. Zhang, X. Fan, (2020). Boosting aqueous zinc-ion storage in MoS_2 via controllable phase, Chemical Engineering Journal 389, 124405. https://doi.org/10.1016/j.cej.2020.124405

[35] S.S. Sinha, L. Yadgarov, S.B. Aliev, Y. Feldman, I. Pinkas, P. Chithaiah, S. Ghosh, A. Idelevich, A. Zak, R. Tenne, (2021). MoS_2 and WS_2 nanotubes: Synthesis, structural elucidation, and optical characterization, The Journal of Physical Chemistry C 125, 6324-6340. https://doi.org/10.1021/acs.jpcc.0c10784

[36] H. Lin, X. Chen, H. Li, M. Yang, Y. Qi, (2010). Hydrothermal synthesis and characterization of MoS_2 nanorods, Materials Letters 64, 1748-1750. https://doi.org/10.1016/j.matlet.2010.04.032

[37] D.T.T. Ngan, V.T. Thuy, D. Van Tuan, N.D. Dien, P.D. Tam, (2025). MoS_2/Ag Composite-Based Biosensor with Improved Sensitivity and Selectivity for Glucose Detection, Journal of Electronic Materials 54, 3981-3993. https://doi.org/10.1007/s11664-025-11846-2

[38] L. Cai, J. He, Q. Liu, T. Yao, L. Chen, W. Yan, F. Hu, Y. Jiang, Y. Zhao, T. Hu, (2015). Vacancy-induced ferromagnetism of MoS_2 nanosheets, Journal of the American Chemical Society 137, 2622-2627. https://doi.org/10.1021/ja5120908

[39] S. Jayabal, J. Wu, J. Chen, D. Geng, X. Meng, (2018). Metallic 1T-MoS_2 nanosheets and their composite materials: Preparation, properties and emerging applications, Materials Today Energy 10, 264-279. https://doi.org/10.1016/j.mtener.2018.10.009

[40] S.A. Getaneh, A.G. Temam, G.A. Workneh, A.C. Nwanya, P.M. Ejikeme, F.I. Ezema, (2024). Advances in MoS_2-Based ternary nanocomposites for high-performance electrochemical energy storage, Hybrid Advances 7, 100333. https://doi.org/10.1016/j.hybadv.2024.100333

[41] P. Kour, S. Kour, A. Sharma, K. Yadav, (2023). MoS_2-based core-shell nanostructures: Highly efficient materials for energy storage and conversion applications, Journal of Energy Storage 66, 107393. https://doi.org/10.1016/j.est.2023.107393

[42] X. Liu, X. Zhang, S. Ma, S. Tong, X. Han, H. Wang, (2020). Flexible amorphous MoS_2 nanoflakes/N-doped carbon microtubes/reduced graphite oxide composite paper as binder free anode for full cell lithium ion batteries, Electrochimica Acta 333, 135568. https://doi.org/10.1016/j.electacta.2019.135568

[43] Y. Wang, B. Chen, D.H. Seo, Z.J. Han, J.I. Wong, K.K. Ostrikov, H. Zhang, H.Y. Yang, (2016). MoS_2-coated vertical graphene nanosheet for high-performance rechargeable lithium-ion batteries and hydrogen production, NPG Asia

Materials 8, 268. https://doi.org/10.1038/am.2016.44

[44] Z. Lei, X. Yu, Y. Zhang, J. Zhan, (2021). Thermally stable fishnet-like 1T-MoS_2/CNT heterostructures with improved electrode performance, Journal of Materials Chemistry A 9, 4707-4715. https://doi.org/10.1039/D0TA10812J

[45] S. Suganya, G. Janani, M. Aparna, S. Sambasivam, K. Yusuf, F. Ran, S. Sudhahar, (2025). Exploration of MoS_2 nanoflowers on g-C_3N_4 nanosheets as a cathode electrode material for hybrid supercapacitor applications, Electrochimica Acta 513, 145595. https://doi.org/10.1016/j.electacta.2024.145595

[46] C. Wang, C. Zhan, X. Ren, R. Lv, W. Shen, F. Kang, Z.-H. Huang, (2019). MoS_2/carbon composites prepared by ball-milling and pyrolysis for the high-rate and stable anode of lithium ion capacitors, RSC Advances 9, 42316-42323. https://doi.org/10.1039/C9RA09411C

[47] D.N. Sangeetha, M.S. Santosh, M. Selvakumar, (2020). Flower-like carbon doped MoS_2/Activated carbon composite electrode for superior performance of supercapacitors and hydrogen evolution reactions, Journal of Alloys and Compounds 831, 154745. http://dx.doi.org/10.1016/j.jallcom.2020.154745

[48] T. Sun, Z. Li, X. Liu, L. Ma, J. Wang, S. Yang, (2017). Oxygen-incorporated MoS_2 microspheres with tunable interiors as novel electrode materials for supercapacitors, Journal of Power Sources 352, 135-142. https://doi.org/10.1016/j.jpowsour.2017.03.123

[49] M. Manuraj, K.V.K. Nair, K.N.N. Unni, R.B. Rakhi, (2020). High performance supercapacitors based on MoS_2 nanostructures with near commercial mass loading, Journal of Alloys and Compounds 819, 152963. https://doi.org/10.1016/j.jallcom.2019.152963

[50] R. Palanisamy, D. Karuppiah, S. Venkatesan, S. Mani, M. Kuppusamy, S. Marimuthu, A. Karuppanan, R. Govindaraju, S. Marimuthu, S. Rengapillai, (2022). High-performance asymmetric supercapacitor fabricated with a novel MoS_2/Fe_2O_3/Graphene composite electrode, Colloid and Interface Science Communications 46, 100573. https://doi.org/10.1016/j.colcom.2021.100573

[51] C. Qu, J. Cao, Y. Chen, M. Wei, H. Fan, X. Liu, X. Li, Q. Wu, B. Feng, L. Yang, (2023). In-situ growth of hierarchical trifunctional Co_4S_3/Ni_3S_2@MoS_2 core-shell nanosheet array on nickel foam for overall water splitting and supercapacitor, International Journal of Hydrogen Energy 48, 648-661. https://doi.org/10.1016/j.ijhydene.2022.09.278

[52] S. Kumar, G. Saeed, L. Zhu, K.N. Hui, N.H. Kim, J.H. Lee, (2021). 0D to 3D carbon-based networks combined with pseudocapacitive electrode material for high energy density supercapacitor: A review, Chemical Engineering Journal 403, 126352. https://doi.org/10.1016/j.cej.2020.126352

[53] J. Wei, G. Li, J. Tong, C. Li, (2025). NH_2@MoS_2 impregnated MXene adsorbents for eliminating cationic dyes: Insight into pH, ionic strength and adsorption mechanism, Diamond and Related Materials 159, 112883. https://doi.org/10.1016/j.diamond.2025.112883

[54] H.J. Song, S. You, X.H. Jia, J. Yang, (2015). MoS_2 nanosheets decorated with magnetic Fe_3O_4 nanoparticles and their ultrafast adsorption for wastewater treatment, Ceramics International 41, 13896-13902. https://doi.org/10.1016/j.ceramint.2015.08.023

[55] Y. Zhang, S. He, Y. Zhang, Y. Feng, Z. Pan, M. Zhang, (2022). Facile synthesis of PPy@MoS_2 hollow microtubes for removal of cationic and anionic dyes in water treatment, Colloids and Surfaces A: Physicochemical and Engineering Aspects 632, 127765. https://doi.org/10.1016/j.colsurfa.2021.127765

[56] K. Ai, C. Ruan, M. Shen, L. Lu, (2016). MoS_2 nanosheets with widened interlayer spacing for high-efficiency removal of mercury in aquatic systems, Advanced Functional Materials 26, 5542-5549. https://doi.org/10.1002/adfm.201601338

[57] J. Joy, J. Abraham, J. Sunny, J. Mathew, S.C. George, (2020). Hydrophobic, superabsorbing materials from reduced graphene oxide/MoS_2 polyurethane foam as a promising sorbent for oil and organic solvents, Polymer Testing 87, 106429. https://doi.org/10.1016/j.polymertesting.2020.106429

[58] Z.H. Jabbar, B.H. Graimed, S.H. Ammar, D.A. Sabit, A.A. Najim, A.Y. Radeef, A.G. Taher, (2024). The latest progress

in the design and application of semiconductor photocatalysis systems for degradation of environmental pollutants in wastewater: Mechanism insight and theoretical calculations, Materials Science in Semiconductor Processing 173, 108153. https://doi.org/10.1016/j.mssp.2024.108153

[59] J. Aliaga, N. Chamorro, M. Alegría, J.F. Araya, F. Paraguay-Delgado, G. Alonso-Núñez, G. González, E. Benavente, (2025). Rhenium-doped MoS_2 3D-flower-like nanosheets on 2D-TiO_2 core-shell for synergistic photocatalytic degradation of RhB under visible light, Materials Today Communications 44, 111961.
https://doi.org/10.1016/j.mtcomm.2025.111961

[60] S. Abdu, H.Y. Hafeez, J. Mohammed, A.A. Safana, C.E. Ndikilar, A.B. Suleiman, I. Alfa, (2025). Advances and challenges in MoS_2-based photocatalyst for hydrogen production via photocatalytic water splitting, Materials Today Sustainability 31, 101142. https://doi.org/10.1016/j.mtsust.2025.101142

[61] Y. Yang, L. Wei, S. Luo, X. Yang, (2025). High-efficiency PPy@MoS_2 core-shell heterostructure Photocatalysts for enhanced pollutant degradation activity, Results in Chemistry 14, 102091.
https://doi.org/10.1016/j.rechem.2025.102091

[62] D.D. La, D.N. Vu, M. Tonezzer, S.V. Bhosale, D. Van Lai, S.S. Kim, D.D. Nguyen, (2025). Porphyrin-MoS_2 hybrid nanostructure: A self-assembled photocatalyst for enhanced organic dye degradation, Surfaces and Interfaces 72, 107143. https://doi.org/10.1016/j.surfin.2025.107143

[63] Y. Bai, G. Jia, (2025). Efficient selective separation of dyes by TA-MoS_2/calcium silicate hydrate composite filtration system, Journal of Physics and Chemistry of Solids 206, 112864.
https://doi.org/10.1016/j.jpcs.2025.112864

[64] M. Abazari, H. Mahdavi, (2022). Synthesis and application of MoS_2 quantum dots-decorated ZnO nanoparticles for the fabrication of loose nanofiltration membranes with improved filtration, anti-fouling, and photocatalytic performance, Chemical Engineering Research and Design 185, 391-406.
https://doi.org/10.1016/j.cherd.2022.07.026

[65] Z. Al Ansari, L.F. Vega, L. Zou, (2024). Emulsified oil fouling resistant cellulose acetate-MoS_2-nanocomposite membrane for oily wastewater remediation, Desalination 575, 117335.
https://doi.org/10.1016/j.desal.2024.117335

[66] Z.C. Elidrissi, A. Essate, B. Achiou, S. Rode, B. Belaissaoui, S.A. Younssi, M. Ouammou, (2025). High-performance MoS_2-based composite membrane for efficient dye/salt separation in textile industry, Separation and Purification Technology 376, 133901. https://doi.org/10.1016/j.seppur.2025.133901

[67] F.G. Afra, H. Hamidinezhad, H. Mozafari, (2025). Antibacterial Activity of Two-Dimensional MoS2 Nanostructures: Effects of Reaction Time and Temperature on Morphology, Materials Chemistry and Physics 343, 130945. https://doi.org/10.1016/j.matchemphys.2025.130945

[68] B. Konwar, S. Kashyap, S. Raghavan, K.-s. Kim, (2025). Alpha to omega for molybdenum disulfide (MoS_2)-based antibacterial nanomaterials, International Journal of Pharmaceutics 675, 125531.
https://doi.org/10.1016/j.ijpharm.2025.125531

[69] H. Ganesha, S. Veeresh, Y.S. Nagaraju, M. Vandana, M. Basappa, H. Vijeth, H. Devendrappa, (2022). 2-Dimensional layered molybdenum disulfide nanosheets and CTAB-assisted molybdenum disulfide nanoflower for high performance supercapacitor application, Nanoscale Advances 4, 521-531.
https://doi.org/10.1039/D1NA00664A

[70] Q. Mao, K. Wei, T. Li, J. Zhu, H. Han, K. Hu, C. Ma, S. Feng, (2025). S-Scheme WO_{3-x}/MoS_2 Heterojunction Photocatalysis coupling with Micro-Nano Bubbles Technology for Enhanced Antibacterial Disinfection in Water, Environmental Research 286, 122966. https://doi.org/10.1016/j.envres.2025.122966

[71] C. Liu, Y. Li, W. Li, Y. Fan, W. Zhou, C. Xiao, P. Yu, Y. Liu, X. Liu, Z. Huang, (2024). LSPR-enhanced photoresponsive antibacterial efficiency of Bi/MoS_2-loaded fibrin gel for management of diabetic wounds, International Journal of Biological Macromolecules 277, 134430. https://doi.org/10.1016/j.ijbiomac.2024.134430